RESEARCH ARTICLE

Fragmentation behavior of young pyroclasts from Mt. Pelée, Martinique

Mila Huebsch[1,2] · Ulrich Kueppers[1] · Guillaume Carazzo[3] · Corrado Cimarelli[1] · Kai-Uwe Hess[1] · Adrian Hornby[4] · Anne-Marie Lejeune[5,6] · Audrey Michaud-Dubuy[3,7] · Diego Perugini[8] · Daniel Weller[1] · Michael J. Heap[9,10] · Donald B. Dingwell[1]

Abstract

The stratovolcano Mt. Pelée, Martinique, exhibits eruptive styles ranging from dome formation to sustained, highly violent explosive activity. Historical eruptions have produced lava domes and pyroclastic density currents, collectively termed Peléan activity. In pre-colonial times, several Plinian eruptions took place. Here, we explore physical controls on the proportions of fine particles produced—i.e., the fragmentation efficiency—during primary fragmentation. Samples were collected from ignimbrites from the 1929–1932 and 1902–1905 Peléan eruptions and the P1 (1300 CE), P2 (280 CE), and P3 (79 CE) Plinian eruptions. All samples are andesitic in bulk composition and contain a rhyolitic groundmass glass. The Peléan materials are more crystalline and less porous than their Plinian counterparts, a consequence of more extensive outgassing during dome formation. Representative blocks were cored and experimentally fragmented following rapid decompression (> 1 GPa·s^{-1} from initial pressure between 5 and 20 MPa). Dry sieving allowed for determining grain size distributions, from which the fractal dimensions, D_f, were calculated as a quantification of fragmentation efficiency. Our results indicate different behaviors for Peléan and Plinian samples. While fragmentation efficiency is positively correlated with applied potential energy for Peléan samples, this relationship is not observed for the Plinian samples, possibly due to syn-fragmentation gas escape above a certain porosity. The rapid decompression experiments were designed to minimize secondary fragmentation by shear along the walls or impact while preserving the entirety of produced materials. Thus, our experimental grainsize data are physically linked to sample textures and overpressure. By comparison with natural pyroclastic products—commonly incompletely preserved—we can approach quantitatively constraining the energetic conditions underlying individual eruptions.

Keywords Eruption style · Magma properties · Grain size distribution · Rapid decompression experiments · Fractal dimension

Introduction

Mt. Pelée has erupted at least 20 times in the past 5000 years (including the devastating eruption of May 8, 1902) and is thus one of the most active volcanoes in the Eastern Caribbean (Westercamp and Traineau 1983; Michaud-Dubuy et al. 2023). Seismic unrest and tremors in 2020, 2021, and 2022 have been interpreted to reflect movements of overpressurized fluids in shallow, subsurface fractures, with much of this movement occurring above sea level (weekly reports throughout 2020–2022 from Observatoire Volcanologique et Sismologique de Martinique). These observations led the local volcano observatory to increase monitoring and advise the local authorities to raise the alert level from green (no alert) to yellow (vigilance) in December 2020. Resumption of explosive activity could disperse lapilli and ash across the island, disrupting the lives of the ~385,000 inhabitants (population from Naulin 2016). Additionally, pyroclastic density currents (PDCs) could threaten the re-established town of St. Pierre and other towns, villages, and settlements situated on the flanks of the volcano.

Fragmentation behavior and eruptive styles of recent eruptions have varied significantly, despite magma composition remaining consistent (Dupuy et al. 1985; Fichaut et al.

1989; Martel et al. 1998; Martel and Poussineau 2007). This is likely due to differences in decompression rates, degassing behavior, magmatic volatile content, and mass eruption rates (Wilson et al. 1980; Neri and Dobran 1994; Villemant and Boudon 1999; Martel et al. 1998, 2000; Carazzo et al. 2008; Michaud-Dubuy et al. 2018, 2020). Field volcanologists aim to determine the total grain size distribution (TGSD) of pyroclastic deposits of unobserved eruptions as an indicator of fragmentation efficiency and eruption energy, both of which positively influence the production of fine particles (Turcotte 1986, 1992; Kaminski and Jaupart 1998; Perugini and Kueppers 2012). As the proportion of fine particles increases, so does heat transfer efficiency, consequentially enhancing ash plume rise and PDC mobility. There are several approaches to integrate the grain size distribution (GSD) at individual outcrops in order to estimate the TGSD (e.g., Bonadonna and Houghton 2005 and Costa et al. 2016). All methods are sensitive to the number of outcrops, their spatial distribution, and their distance from the vent (Costa et al. 2016; Aubry et al. 2021). For eruptions with detailed direct observations, there exist only a small number of studies that include TGSD analysis (e.g., Costa et al. 2016; Reckziegel et al. 2016; Pioli et al. 2019). Calculating TGSD from explosive eruption deposits on volcanic islands, like Martinique, is additionally complicated as substantial portions of the eruptive products have been deposited into the ocean and are not preserved in the subaerial rock record (Kueppers et al. 2019). On small islands, field-based approaches to evaluate TGSD based on grain size characteristics (and not thickness alone) have yet to be validated. Moreover, unconsolidated pyroclastic deposits can undergo considerable post-eruption erosion by low-energy and/or short-term processes, such as runoff from rainfall.

Laboratory studies provide insights into primary magma fragmentation with minor to negligible loss of fines, secondary fragmentation, and transport-induced sorting. As rapid decompression drives magma into brittle fragmentation (Dingwell 1996), the resulting GSDs exhibit scale-invariant fractal properties (Turcotte 1992; Korvin 1992; Åstrom et al. 2004), whereby a power-law relationship describes the fragment size distribution in a logarithmic plot of cumulative particles (as in Gilvarry and Bergstrom 1961; Åstrom et al. 2004; Perugini and Kueppers 2012; Haug et al. 2013; Colò et al. 2020; Sarkar et al. 2020). Quantification of the fragmentation efficiency as a single variable (D_f), the fractal dimension, is thus enabled, and a comprehensive comparison across experimental conditions becomes feasible. This can also be applied to field TGSD results, yet a lack of fractal analyses of young explosive deposits currently hinders this approach. For such quantification, either numbers of particles (i.e., fragments) or a mass-based approach is used, both of which summarize the fractal change in the amount of fragments generated for incremental size steps.

When numbers of particles are analyzed for fractal distribution, following the initial mathematical methodology of Mandelbrot (1983) and Turcotte (1989), particle shape is commonly assumed to be spherical (e.g., Kaminski and Jaupart 1998 and Kueppers et al. 2006a). However, pyroclasts exhibit highly irregular geometric shapes, and certain size fractions can deviate very substantially from the spherical assumption (Liu et al. 2015). To avoid this challenge, we follow here the approach of Perugini and Kueppers (2012) in using the cumulative weight fractions for fractal distribution analysis. Assuming that the volume of a fragment is proportional to its mass, D_f is derived from the size-mass relationship without requiring any information or assumptions regarding shape.

Following petrophysical characterization and experimental fragmentation of natural samples from recent Plinian and Peléan eruptions of Mt. Pelée, we evaluate the resulting GSDs and explore controls on the fragmentation behavior. We thereby aim to advance our understanding of how sample properties can influence fragmentation efficiency and consequently eruption dynamics. This information will help to refine tools for relating physical properties of pyroclastic deposits and individual clasts to past eruption dynamics, a necessary element of determining what eruption styles and intensity volcanoes are capable of.

Geologic setting

Mt. Pelée volcano forms the northern part of the island of Martinique, in the Eastern Caribbean. It is part of an oceanic arc forming on the Caribbean plate due to westward-directed subduction of the South American plate, at a rate of about 1.3–4 cm year^{-1} (Macdonald et al. 2000). The volcanic formation of Martinique began as early as 40 Ma (Brown et al. 1977; Smith and Roobol 1990), with activation of several volcanic centers over time. The active volcanic center moved to the northern end of the island around 550 ka and built Mount Conil, located to the northwest of the most recent vent (Germa et al. 2015). During the next ~425 ky, the eruptive activity produced andesitic lava flows, lava domes, and variably welded pyroclastic flows (Westercamp and Traineau 1983; Germa et al. 2011). Following a large flank collapse at ~127 ka (Le Prêcheur event: Le Friant et al. 2003; Brunet et al. 2016), the Paleo-Pelée cone formed in the preserved northern rim of the flank-collapse structure (Vincent et al. 1989). This more explosive phase of growth produced alternating pumice falls, pumice, and/or scoria flows and block-and-ash flows until ~36 ka (Solaro et al. 2020). In the past 2 ka, Mt. Pelée has exhibited alternating Plinian and Peléan type behavior (Westercamp and Traineau 1983; Vincent et al. 1989; Boudon et al. 2005), the latter of which involves dome formation and small-volume PDCs (Roobol and Smith 1976).

In this study, we focused on five of the most recent magmatic eruptions, which took place in 1929–1932 CE (referred to as 1929), 1902–1904 CE (referred to as 1902), ca. 1300 CE (P1), ca. 280 CE (P2), and ca. 79 CE (P3) (Westercamp and Traineau 1983; Traineau et al. 1989; Boudon et al. 2005). The twentieth century eruptions were Peléan, in that they produced lava domes and dilute PDCs, while the earlier three eruptions were primarily Plinian, producing interspersed pumice lapilli fallout and deposits of variably dense PDCs as column stability varied (Westercamp and Traineau 1983; Carazzo et al. 2012, 2019, 2020). The local trade winds result in a generally westward tephra dispersal (Carazzo et al. 2012, 2019, 2020) with local precipitation maxima on the northeastern flanks of Mt. Pelée and a rain shadow in the southwest (Michaud-Dubuy et al. 2019).

Recent history of Mt. Pelée

Archeological artifacts underlying P2 deposits indicate that Martinique was inhabited prior to 280 CE, before being evacuated at the onset of the eruption (e.g., Bérard et al. 2003 and Carazzo et al. 2019). The island was then re-inhabited prior to the beginning of European settlement in 1635 (Bourdier et al. 1989; Smith and Roobol 1990), likely closely following Peléan activity which left the flanks void of vegetation (Westercamp and Traineau 1983). After two minor phreatic eruptions in 1792 and 1851, the first magmatic activity observed on Martinique after European settlement occurred in 1902, preceded by increased fumarolic activity, as well as phreatic and phreatomagmatic eruptions (Bourdier et al. 1989; Smith and Roobol 1990). On May 8, 1902, PDCs overflowed topographic barriers and devastated the town of St. Pierre—amongst other towns and villages—resulting in the deaths of ~28,000 people (Lacroix 1904; Bourdier et al. 1989; Gueugneau et al. 2020). This eruption is considered the deadliest of the twentieth century and may have been the most catastrophic on Martinique. Over the following months, dilute and dense PDCs were observed, as well as growth of a lava dome and eventually the iconic ~350 m high spine (Lacroix 1904; Smith and Roobol 1990). During these events, the town of Morne Rouge was also destroyed, leading to 1500 further deaths (Bourdier et al. 1989). The most recent eruptive activity of Mt. Pelée occurred from 1929 to 1932, including phreatic or phreatomagmatic eruptions, dome formation, and PDCs—deposits of which overlie those from 1902 in a smaller region on the south flank of the volcano (Romer 1934). Products of recent eruptions (i.e., P4 at 2.5 ka and younger) have average silica content of 62 wt.%, forming a bulk andesitic composition, with phenocryst content ranging from 35 to 58 vol.% and rhyolitic matrix glass (Martel et al. 1998).

Consistency in bulk chemical composition and physical conditions across recent eruptions indicates homogeneity of an unchanging magma reservoir source (Martel and Poussineau 2007), with pre-eruptive storage at 875–900 °C, 200±50 MPa, approximate oxygen fugacity of NNO + 0.6, and H_2O contents of 5.3–6.3 wt.% in the melt (Martel et al. 1998). Mafic enclaves with 51–59 wt.% SiO_2 and banded clasts were produced during the 1902 and 1929 eruptions, and minor amounts of inherited phenocrysts grown from mafic melts are present across eruptions, together indicating magma mixing between the primary andesitic reservoir and a distinct mafic source (Fichaut et al. 1989; Gourgaud et al. 1989; Pichavant et al. 2002).

Materials and methods

Sample collection and preparation

During a first sampling campaign in 2013, samples were collected from all volcano flanks. Preliminary experiments (Holzmueller and Kueppers 2015; Kueppers et al. 2015) showed results inconsistent with empirical findings in the same set up (Spieler et al. 2004; Kueppers et al. 2006a, b; Scheu et al. 2006). It was concluded that a follow-up sampling campaign was required to constrain Mt. Pelée's behavior, excluding outcrops from the eastern flanks where precipitation is more substantial. In March 2019, samples were collected from ignimbrites from the 1929, 1902, P1, P2, and P3 eruptions, outcropping in riverbanks and roadside cuts. Outcrop locations are shown in Fig. 1, and representative images of each outcrop are shown in Fig. 2. Juvenile, bomb-sized clasts were selected as starting material to enable the drilling of rock cylinders of 25 mm diameter and 60 mm length for laboratory fragmentation experiments (Kueppers et al. 2006a, b). Upon drilling, the two ends of the cylinders were cut parallel and polished with a saw and lathe, respectively, to minimize surface roughness. Finally, the cylinders were washed and dried for at least 12 h at 80°C.

Petrophysical analysis

Cylinder length (L) and diameter (d) were measured using a digital caliper (precision ± 0.01 mm) to calculate bulk volume (V_B) and cross-sectional area (A). Dry mass (M) was determined using a balance (precision ± 0.0001 g) and then divided by V_B to determine dry bulk density (ρ_B) of each cylinder. The displacement volume (V_S) of cylinders and the solid density (ρ_S) of powdered clasts (milled to < 63 μm, sub-sample name ending in "_P") were determined using a *Quantachrome* helium pycnometer (Ultrapyc 1200e), with a precision of 0.0001 g·cm^{-3}. The following set of equations was used to define open porosity (ϕ_O), total porosity (ϕ_T), and closed porosity (ϕ_C).

Fig. 1 DEM map of Mt. Pelée in the north of Martinique. Outcrop locations relevant to this study are labeled with circles, and the summit crater of Mt. Pelée is indicated with a triangle symbol. Key town locations are indicated with diamond symbols. Map generated using open source QGIS software. Coordinates are in WGS 84-UTM Zone 20 system. The inset shows the location of Martinique in the Caribbean arc. Image modified from Michaud-Dubuy (2019)
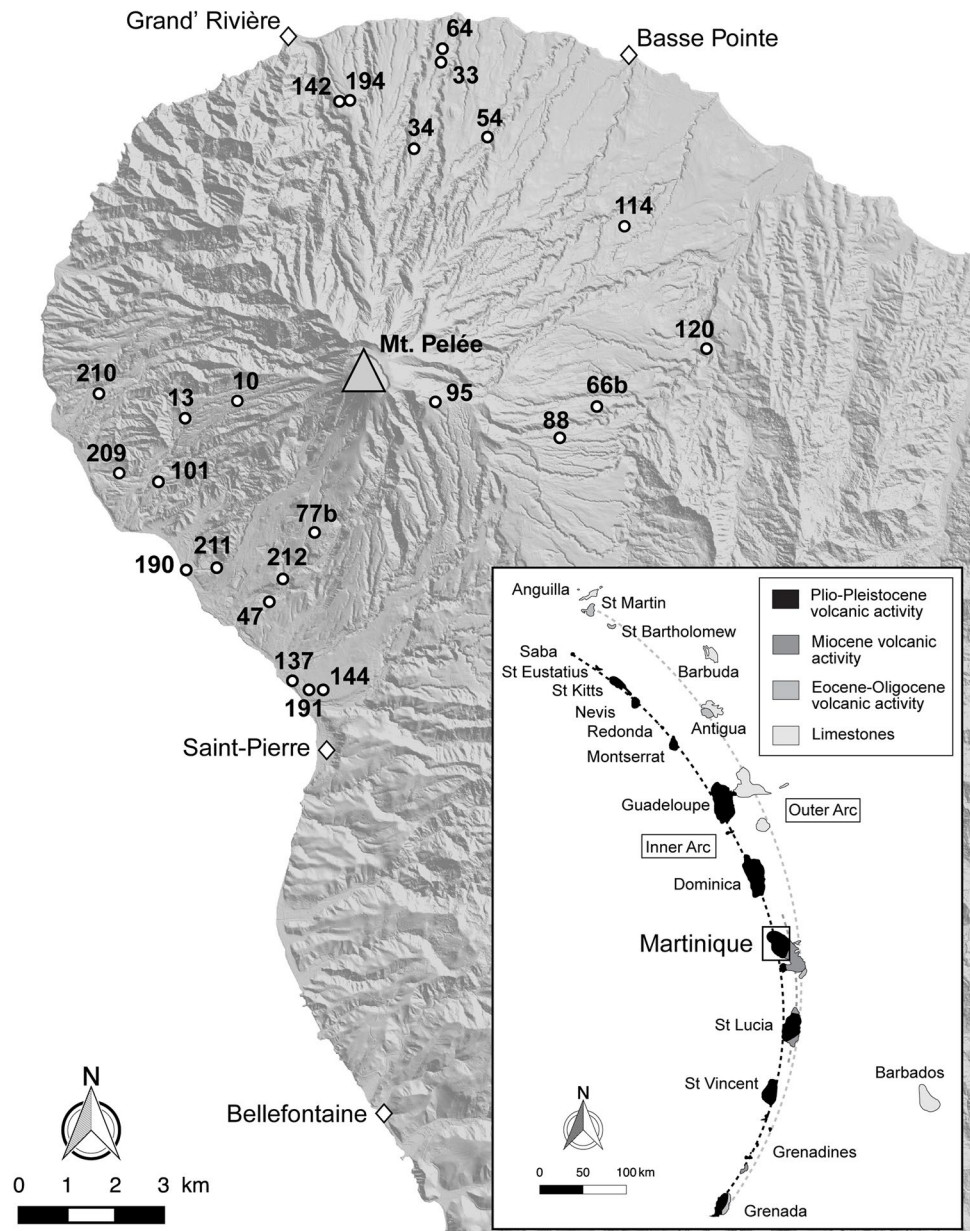
$$\phi_O = \frac{V_B - V_S}{V_B} * 100 \tag{1}$$

$$\phi_T = \frac{\rho_S - \rho_B}{\rho_S} * 100 \tag{2}$$

$$\phi_C = \phi_T - \phi_O \tag{3}$$

Permeability (k_D) was measured for two samples per eruptive unit, using a benchtop gas (nitrogen) permeameter constructed using a quick release coreholder from *Vinci Technologies*, gas flowmeters from *Bronkhorst*, and a pressure transducer from *KELLER* (see Farquharson et al. 2016

and Heap and Kennedy 2016). All permeability measurements were performed at the Strasbourg Institute of Earth and Environment (Strasbourg, France) at ambient laboratory temperature and under a confining pressure of 1 MPa using the steady-state method. One sample (C7-06), which contains rough sidewalls, was wrapped in electrical tape and measured at a confining pressure of 1.5 MPa to ensure that no gas passed between the sample and the jacket. The samples were left to equilibrate microstructurally to the confining pressure for 1 h prior to measurement. Steady-state volumetric flow rates (Q_v) were then measured (using a gas flowmeter) for six different pore pressure differentials (ΔP_k; measured using a pressure transducer), where P_d and P_m are downstream and mean pore fluid pressure,

Fig. 2 Outcrops of sampled ign-imbrites from the 1929, 1902, P1, P2, and P3 eruptions, in **a** through **e**, respectively. Note shovel in **a**, **c**, and **e**; people for scale in **b**, and jointed clast (~15 cm in diameter) indicated by the red arrow in **d**
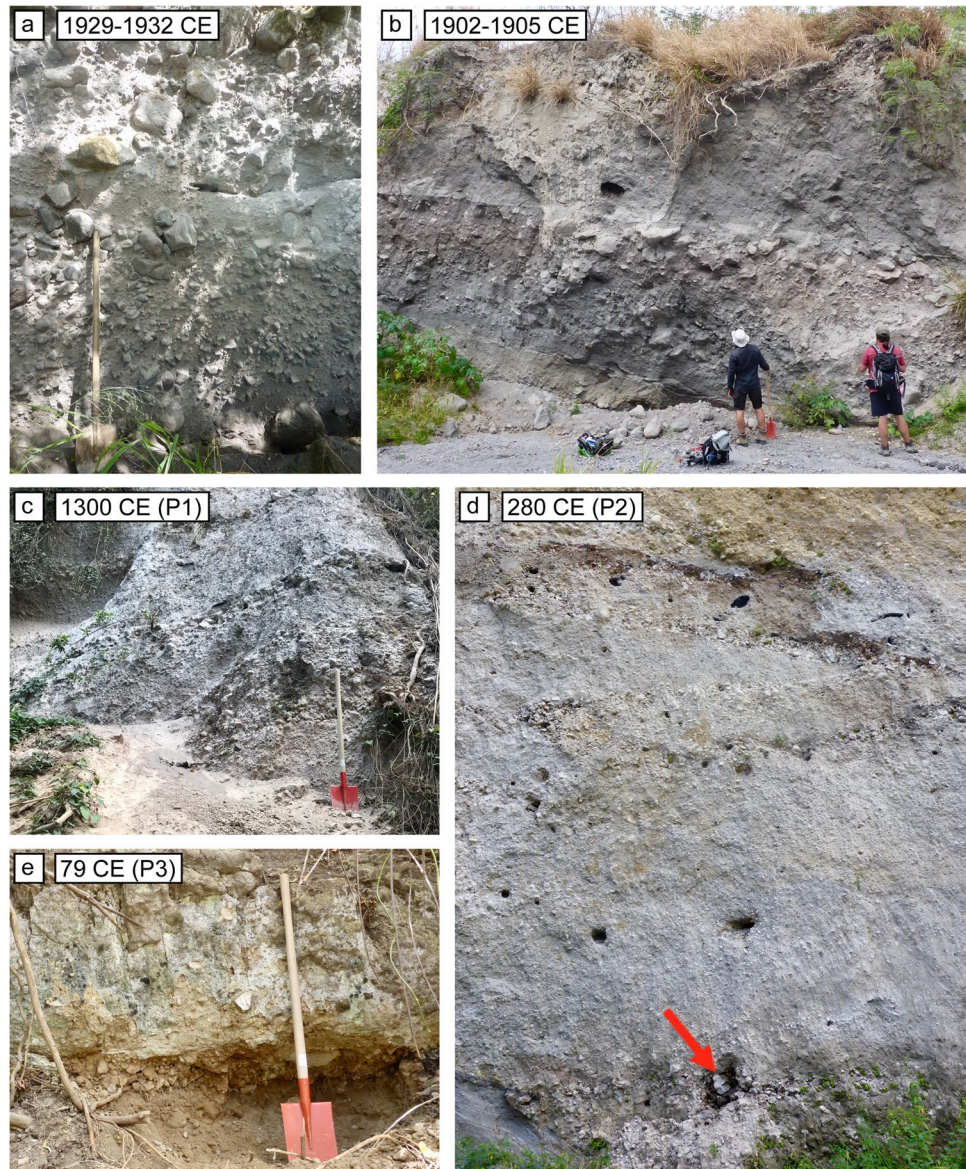
respectively. These data were used to calculate permeability using Darcy's law (Eq. 4) and, where necessary, were corrected using the Klinkenberg or Forchheimer corrections (as in Heap et al. 2017). The viscosity of nitrogen as pore fluid is included as μ.

$$k_D = \frac{Q_v}{P_m \Delta P_k} \frac{\mu L P_d}{A} \tag{4}$$

Textural analysis

Grayscale backscattered electron (BSE) images of representative thick sections of samples from all five eruptions were obtained using a SU5000 Schottky FE-SEM (*Hitachi*) scanning electron microscope (SEM) at the Department of Earth and Environmental Sciences at LMU Munich. Magnification of ×60 to ×1800 was used with an accelerating voltage of 20 kV to observe textural features spanning 5 μm to 2 mm. Approximate phenocryst proportions in each unit were estimated from representative scans using the ImageJ macro RockPie (Hornby 2022), which is based on the ash-surface-salts macro described in Casas et al. (2022). This macro uses user-led grayscale and size thresholding to differentiate void space, glass, and crystals and then performs an area-based calculation to determine areas and proportions of each differentiated component.

Geochemical analysis

The bulk (whole rock) chemical compositions of the volcanic ashes were determined with X-ray fluorescence (XRF) at the Institute of Geosciences, Johannes Gutenberg University, in Mainz, Germany. For this purpose, ash samples were ground for 5 min in a zirconia ball mill to obtain a fine-grained (<63 μm) powder. Major elements were analyzed by measuring fused glass beads (0.4 g sample, 5.2 g $Li_2B_4O_7$ flux) with a Philips Analytical MagiX PRO. Loss-on-ignition (LOI) was determined by weighing the sample before and after heat treatment for 2 h at 980 °C. Electron probe microanalysis (EPMA), using a Cameca SX100 at LMU Munich, was performed on glass with a defocused beam of 10 μm at a current of 5 nA to account for Na migration, while crystalline material was measured with a focused beam at 20 nA, both at 15 kV accelerating voltage and with 10 s count times. The following standards were used: Si and Na, albite; Al and K, orthoclase; Ca, wollastonite; Mg, periclase; Fe, Fe_2O_3; Cr, Cr_2O_3; Ti, ilmenite; Mn, bustamite; P, apatite; Cl, vanadinite; S, anhydrite; Y, YIG ($Y_3Fe_5O_{12}$); Gd, GdIG ($Gd_3Fe_5O_{12}$); Zr, ZrO_2: and Hf, met. Hf.

Rapid decompression experiments

Fragmentation experiments were originally designed by Alidibirov and Dingwell (1996a, b) to investigate the response of porous magma/rock to rapid decompression and accordingly mimic explosive volcanic (magmatic) eruptions. The force of pressurized gas acting on bubble walls during decompression may cause brittle failure and particle ejection. These controlled and repeatable lab experiments empirically correlate the starting conditions (defined by the user) with the observable features of the produced gas-particle jets (Cigala et al. 2017, 2021; Schmid et al. 2020, 2022) and the generated particle population (Kueppers et al. 2006a; Alatorre-Ibargüengoitia et al. 2011). The experiments of this study were performed at room temperature on cylinders with porosity representative of each eruptive unit, and the specific "fragmentation bomb" setup used is shown in Fig. 3. Experimental conditions are manipulated directly, by varying applied pressure (ΔP) and, indirectly, by selecting samples of different connected porosity. The potential energy of fragmentation (PEF) is calculated as the multiplication of ΔP and connected pore volume ($\phi_O \times V_B$). The model of Spieler et al. (2004) was referenced to select ΔP conditions ranging 6–20 MPa, as to exceed sample fragmentation thresholds and cause complete fragmentation.

Once the intended autoclave pressure (adjusted to 0.1 bar precision) is achieved, the independently controlled pressure in the uppermost chamber is increased to exceed the ΔP stability of the uppermost diaphragm, such that it ruptures, releasing gas into the atmospheric-condition collection tank.

The lower diaphragm(s) then consequently open, facilitating decompression of the overpressurized autoclave downward toward the sample, which is momentarily exposed to a steep pressure gradient. If sample textures (e.g., porosity and permeability) and pressure conditions permit, compressed gas in the open pore space of the cylinder expands, bubble wall strength is exceeded, and the sample fragments. Generated clasts are accelerated upwards by the expanding gas and ejected into the collection tank. A pressure transducer is set to trigger collection of pressure data across the depressurization event, as well as high-speed video footage (recorded with a Phantom V710, sampling rate of 10,000 fps, resolution of 1280 by 600 pixels) of 4 s following diaphragm rupture. These videos show decompression to occur in less than 0.1 s. The experimental conditions achieved are summarized in Table 1.

Grain size distribution determination

Following each rapid decompression experiment, the fragments generated were carefully collected from the tank plate and plexiglass tube using a brush. For each experiment, the weight of all fragments is compared to the respective starting cylinder weight (%) (following insertion into the sleeve) and confirms near-complete recovery of all clasts. Products were then dry sieved by hand at half-Φ steps from > 16 mm to < 63 μm diameter, with care to minimize further breaking while obtaining satisfactory size separation. Each size fraction was weighed (precision $\pm$ 0.0001 g) and then stored in a sealed glass vial. The total mass (M_T) of collected products was compared with the collected mass to confirm loss during sieving as << 1 wt.%. In total, we have analyzed the generated clasts of twenty-two experiments performed in this study and seventeen previously performed by Kueppers et al. (2015).

Data analysis

Experimental grain size distributions are analyzed using MATLAB. The base ten logarithm of cumulative weight (CW) fractions for fragments with a linear dimension (r) smaller than each sieve aperture (R) is calculated and plotted against the base ten logarithm of sieve aperture (Φ_{10}). The size range of 250 μm to 4 mm is selected for subsequent calculations, following the reasoning of Perugini and Kueppers (2012) and Sarkar et al. (2020), to account for bias due to the cylinder starting size and possible loss of fine ash. Here, logarithmic cumulative weight fraction plots are examined for linearity within the selected ranges, to establish the fractal character of GSDs. These ranges are then used for a best-fit slope calculation, performed with the MATLAB curve fitting toolbox, using a linear equation form. Following Perugini and Kueppers (2012), the following equations are employed to quantify fragmentation efficiency as a fractal dimension ($D_{f, CW}$).
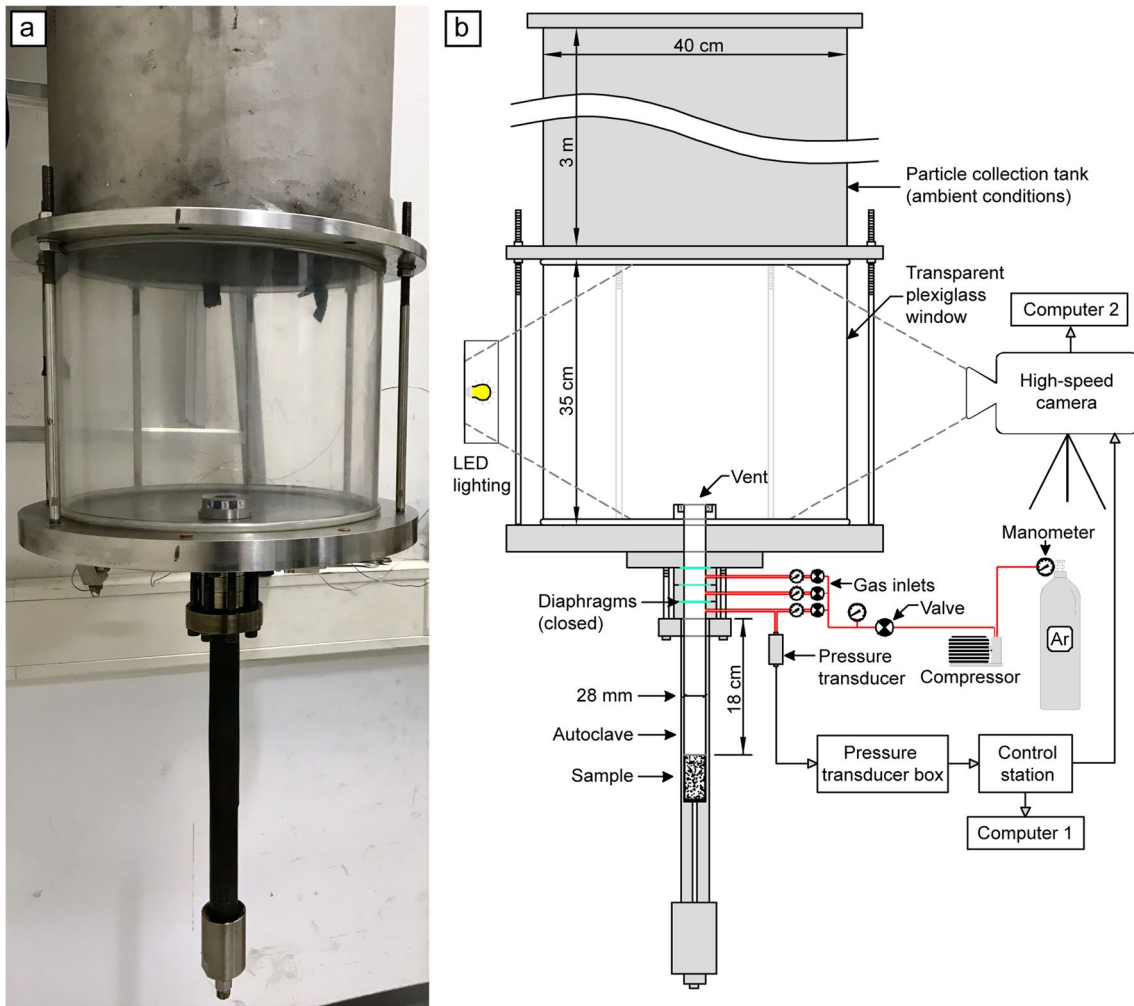
Fig. 3 Photo (left) and schematic (right) of the fragmentation bomb setup for rapid decompression experiments, including from bottom up: sample-containing autoclave, gas inlets, closed diaphragms (blue), tank bottom plate, cylindrical vent, plexiglass window through which high-speed videos are recorded, and the atmospheric pressure collection tank. Gas lines are shown in red, with barometers and valves denoted. Data pathways are denoted by gray-filled arrowheads

$$\frac{M(r < R)}{M_T} = R^v \tag{5}$$

$$D_{f,\mathrm{CW}} = 3 - v \tag{6}$$

Results

Petrophysical properties

All samples from the three Plinian eruptions have a dry bulk density (ρ_B) < 1000 kg m^{-3} and are called pumices from now on, while all Peléan samples exhibit higher and more variable values of bulk and powder density. The pumiceous sub-sample ϕ_O averages range from 55 to 66%, with greater variation between cylinders from separate clasts than for cylinders drilled from the same source clasts (Fig. 4). P3 and P2 clasts collected in 2013 from outcrops 114 and 95, respectively, on the wet, eastern flanks show the greatest sub-sample variability. The 1929 samples have the lowest analyzed ϕ_O, averaging around 32%, while the average ϕ_O of the 1902 samples ranges from 36 to 47%: the widest range for the eruptive units considered. The pumiceous samples have ϕ_C around 10%, whereas the 1902 samples average below 0.5% (such that corresponding ϕ_T tends to be within error of ϕ_O) and the 1929 samples have a ϕ_C of ca. 1%. Permeability values range from 9.89×10^{-13} to 8.00×10^{-12} m^2, without systematic trends across units. The results for Peléan and Plinian samples fit within the effusive and explosive product envelopes as defined for porosity-permeability

Table 1 Experimental conditions, organized by eruptive unit from youngest to oldest. Samples with names starting with a letter were collected in 2019, those with numbers in 2013 (Kueppers et al. 2015). The experimental conditions are manipulated by applying pressure (ΔP) to representative sub-sample cylinders drilled from blocks from each eruption, with varying open porosity (ϕ_O) within their bulk volume (V_B), to create resulting potential energy of fragmentation (PEF). The resulting fragmentation efficiency is quantified from cumulative weight fractions as the fractal dimension, $D_{f,CW}$. Additional parameters are provided in the Supplementary Information (Huebsch et al. 2023)

Eruptive unit	Sub-sample	ΔP (MPa)	ϕ_O (%)	V_B (cm^3)	PEF (J)	$D_{f,\,CW}$
1929	D1_05	10.2	34.95	31.44	112.08	2.31
	D1_01	15.0	30.93	31.44	145.88	2.36
	D2_01	19.6	31.86	31.47	196.52	2.39
1902	C7_05	7.5	47.56	31.16	111.17	2.39
	C7_01	10.2	47.39	31.09	150.28	2.48
	C7_02	15.1	46.20	31.31	218.39	2.44
	C6_04	15.2	35.92	31.66	172.85	2.51
	C6_05	17.1	35.86	31.59	193.74	2.48
	C6_03	20.3	35.72	31.11	225.58	2.51
P1	B1_09	7.9	60.33	31.44	149.84	2.24
	B1_05	10.1	60.27	31.19	189.84	2.22
	B1_07	14.1	60.73	31.55	270.17	2.25
	B1_04	17.6	60.12	31.53	333.61	2.22
	B1_06	20.2	59.79	31.31	378.17	2.17
	77b_01	5	56.61	30.95	87.61	2.30
	77b_02	10	56.92	30.48	173.50	2.30
	77b_03	10	57.20	29.72	169.99	2.34
	77b_04	15	56.77	30.60	260.61	2.31
	77b_05	15	56.85	30.66	261.47	2.32
P2	H1_01	7.4	62.67	30.72	142.45	2.43
	H1_07	10.1	63.10	30.97	197.36	2.41
	H1_06	15.1	63.46	31.00	297.05	2.36
	H1_04	20.1	65.07	30.76	402.38	2.44
	95_06	5	65.94	30.70	101.22	2.55
	95_07	7.5	65.53	30.64	150.61	2.48
	95_01	10	59.19	30.54	180.74	2.25
	95_02	10	60.53	30.18	182.68	2.45
	95_08	15	60.00	30.48	274.34	2.35
	95_09	15	60.57	30.83	280.14	2.21
P3	A1_02	6.7	60.08	31.24	125.73	2.38
	A1_01	10.4	60.20	31.08	194.58	2.28
	A2_02	12.5	58.17	30.81	224.03	2.23
	A2_01	20.2	57.73	31.45	366.81	2.23
	114_04	5	68.82	29.95	103.06	2.56
	114_16	5	67.38	30.87	104.00	2.57
	114_23	10	67.69	30.78	208.35	2.52
	114_07	10	67.58	30.07	203.21	2.47
	114_12	15	64.88	30.49	296.73	2.41
	114_17	15	65.20	30.76	300.83	2.45

combinations by Mueller et al. (2005), respectively. Full petrophysical results can be found in the Supplementary Information (Huebsch et al. 2023).

Textural overview

BSE scans for the Plinian (Fig. 5) and Peléan (Fig. 6) samples highlight strong textural differences. The Plinian samples are highly vesiculated and have a well-connected porosity structure, while the Peléan samples are significantly less vesicular. All observed samples are porphyritic, and in most samples, the phenocrysts of plagioclase and pyroxene are fractured (Figs. 5 and 6). The groundmass of all Peléan samples contains abundant plagioclase microlites (Fig. 6b, d).

Two-dimensional crystal content and void space, respectively, are about 25–30% and 20–40% for the Peléan samples and 10–20% and 50–70% for the Plinian samples, in good agreement with pycnometry results. Most vesicles in the Plinian samples are round with a low aspect ratio, indicative of rapid vesiculation, while the heterogeneous orientation of

Fig. 4 Pycnometry porosity data for each analyzed sub-sample, organized by parent sample and eruptive unit, from oldest (P3, left) to youngest (1929, right). Standard error smaller than symbol size. Open symbols correspond to data from Kueppers et al. (2015)
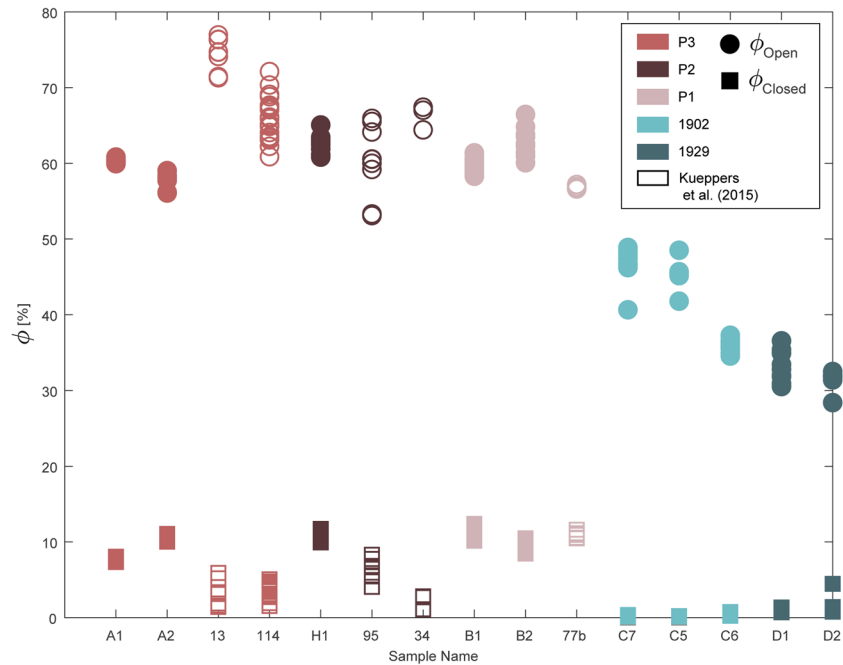
the longest axis indicates localized regions of ductile deformation (Fig. 5d). The Peléan samples on the contrary exhibit irregularly shaped vesicles and a lower bubble number density (Fig. 6), following coalescence and outgassing.

Geochemistry

Bulk XRF analysis confirms that the erupted products from the five considered eruptions are andesitic, with no systematic silica or alkali trend across units (Fig. 7). Electron microprobe data, shown alongside results of Martel and Poussineau (2007), indicates that all measured glasses are rhyolitic, with greater variability in the denser, Peléan samples due to increased microlite content (Fig. 7). Spot analysis of phenocrysts show plagioclase to be primarily bytownite, ranging from labradorite to anorthite (An_{65-95}), and orthopyroxene to be hypersthene, intermediate in ferrosilite content (Fs_{50-60}).

Experimental grain size distributions

All fragmentation experiments led to complete disintegration of the starting cylinders. GSD results are shown in Fig. 8 and show distinct responses for Plinian and Peléan samples to rapid decompression. The mode (i.e., peak location and shape) remained largely constant per sample set, and no strong positive correlation was observed between starting experimental pressure and the weight fraction of fine particles ($\Phi_2 < 0$) created. Results for P1, P2, and P3 show mono-modal peaks between $\Phi_2 \approx -1$ and $\Phi_2 \approx -1.5$. Weight fraction results for 1902 and 1929 experiments form

a broader peak around $\Phi_2 \approx -1$ and $\Phi_2 \approx 0.5$. Sub-millimeter proportions of all produced fragments for 1902 and 1929 experiments were 51 wt.% and 34 wt.%, respectively, and 25 wt.%, 25 wt.%, and 30 wt.% for the P1, P2, and P3 experiments, respectively. Additionally, the fractal behavior has been investigated for each data set between 2.8 mm and 250 µm (vertical dashed lines in Fig. 8). The results show the dependence of $D_{f,\,CW}$ on PEF for the Peléan samples only (Fig. 9) and confirm the observed separation of the five investigated sample sets into two distinct groups. A generally positive trend exists for the Peléan (1902 and 1929) samples, whereas for the Plinian (P1, P2, P3) samples, fragmentation efficiency did not increase systematically with PEF.

Discussion

Magma characteristics

Our geochemical results confirm the findings of Martel and Poussineau (2007) that the volumetrically dominant magmas at the source of the 1929, 1902, P1, P2, and P3 eruptions are compositionally very similar (Fig. 7). This indicates that the magma reservoir compositionally unchanged over at least the last 2000 years. Textural heterogeneities between eruption units, excluding the minor mafic enclave content observed, likely correspond to variations in ascent conditions and eruption dynamics associated with the Plinian and Peléan eruptive styles. We note here, however, that our study materials are, of necessity, all similarly sized pyroclastic bombs. These were selected for drilling multiple
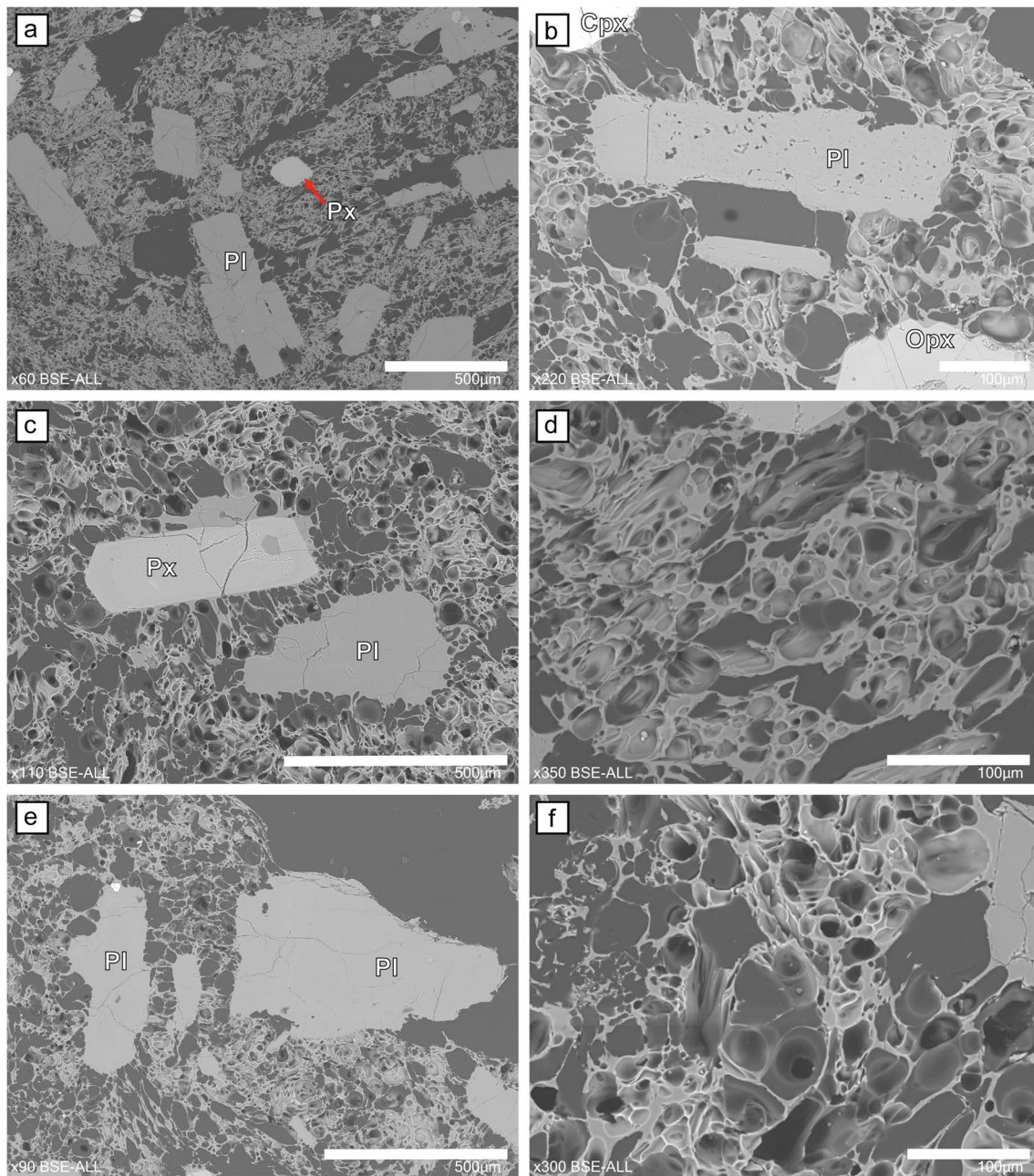
Fig. 5 Back-scattered electron (BSE) images of the Plinian samples, deriving from the P3 (**a**, **b**), P2 (**c**, **d**), and P1 (**e**, **f**) eruptions. Two phenocryst populations can be observed: plagioclase (darker gray) and pyroxene (slightly brighter gray), as labeled. All samples exhibit high bubble number density. The scale bars in the left- and right-hand overview and zoom sub-figures are 500 μm and 100 μm long, respectively

experimental cylinders from each, and thus, their characteristics cannot represent eruption phases where such products are absent.

The strong contrast in microlite contents (Figs. 5 and 6) indicates substantial differences in cooling history between the Peléan and Plinian source magmas, with faster decompression and cooling (and accordingly less crystallization) in the latter. This requires substantially higher ascent velocities for the "Plinian magmas," causing stronger oversaturation and, in the near absence of microlites, faster volume increase following homogeneous bubble nucleation. Thus, the limited time for outgassing facilitates significant overpressure build-up. In the Peléan cases, slower magma ascent and dome extrusion enabled efficient outgassing and related microlite nucleation and growth (Toramaru et al. 2008). Our observation of major

Fig. 6 Back-scattered electron (BSE) images of samples from 1902 (**a**, **b**) and 1929 (**c**, **d**). Plagioclase microlites appear as bright fine spots in the matrix (**b**, **d**). Exemplary phenocrysts or microlites are labeled in each subfigure, and plagioclase phenocrysts with low contrast to glassy matrix are outlined in white in **d**. The scale bars in the left- and right-hand overview and zoom sub-figures are 500 µm and 100 µm long, respectively
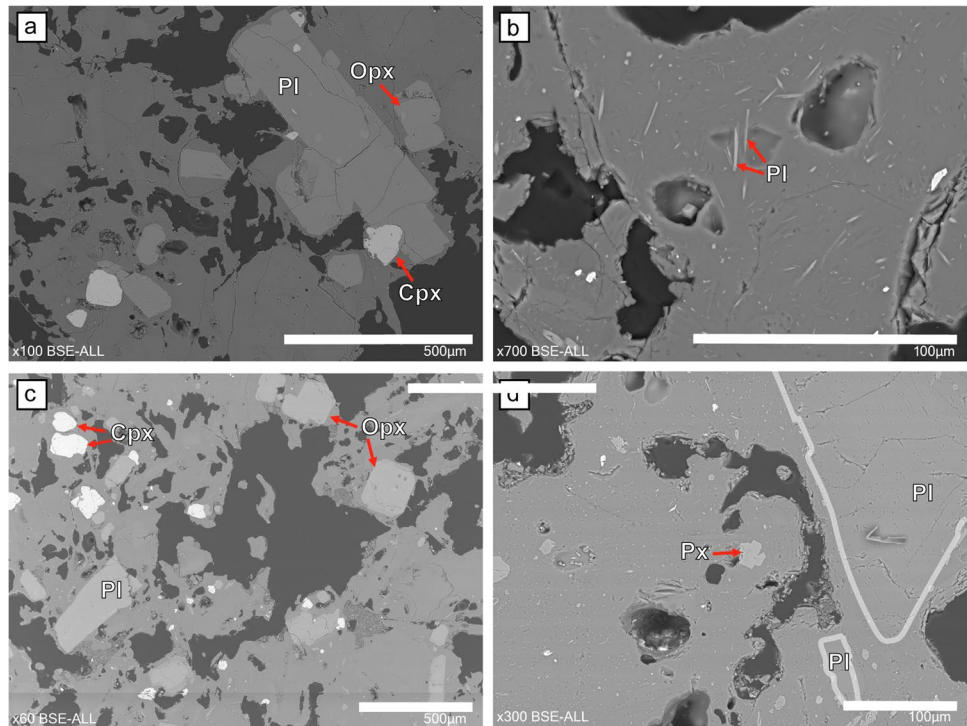
Fig. 7 TAS diagram for results of XRF on representative powdered whole-rock samples (one per unit, with 1% relative error) and EPMA on interstitial glasses (averages of at least four measurements per eruptive unit, with statistical error shown). The ranges of EPMA results and relative error from Martel and Poussineau (2007) are shown as darker and lighter gray fields, respectively
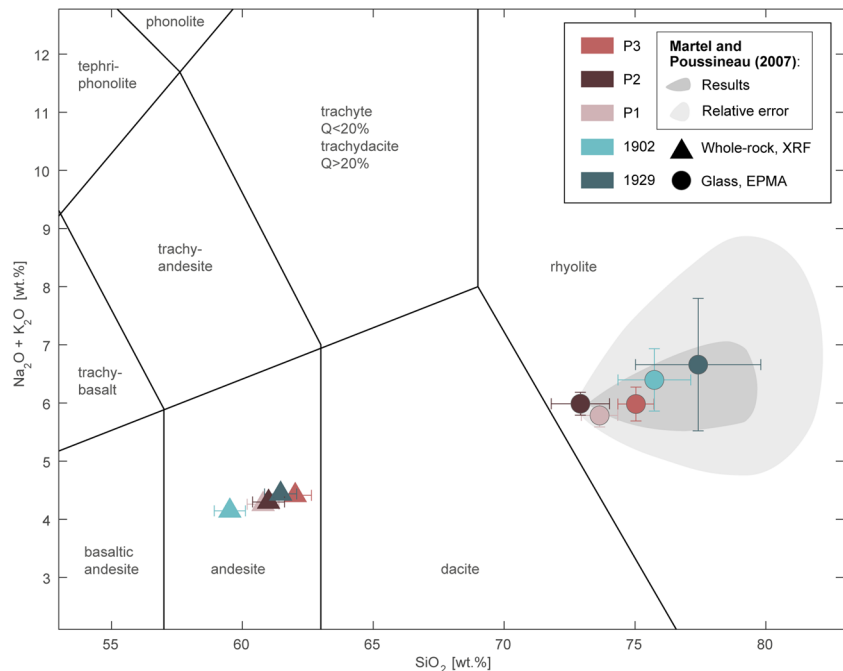
phenocryst content in BSE images, consistent across eruptive units, is in agreement with the results of Gourgaud et al. (1989) and Martel et al. (1998).

In accordance with their different microlite and phenocryst contents, vesicle shapes are irregular in Peléan samples (Fig. 6) and rounder in Plinian samples (Fig. 5), in agreement with the results of Martel et al. (2000) and

Martel and Poussineau (2007). Our textural observations, alongside the H$_2$O contents of ~0.2–1.6 wt.% for 1902 and 1929 samples and ~5.5 wt.% for P1 fallout and PDC samples (assumed to not have experienced post-depositional hydration) reported by Martel et al. (2000), support more thorough outgassing and dehydration during the Peléan eruptions.

Fig. 8 Grain size distributions shown as weight fractions across the negative base-two logarithm of sieve aperture. The left column (**a**, **c**, **e**) and right column (**b**, **d**) show results of fragmentation experiments performed with samples of the Plinian eruptions P3, P2, and P1 and Peléan eruptions 1902 and 1929, respectively. Vertical dashed lines indicate the limits of the analyzed data range
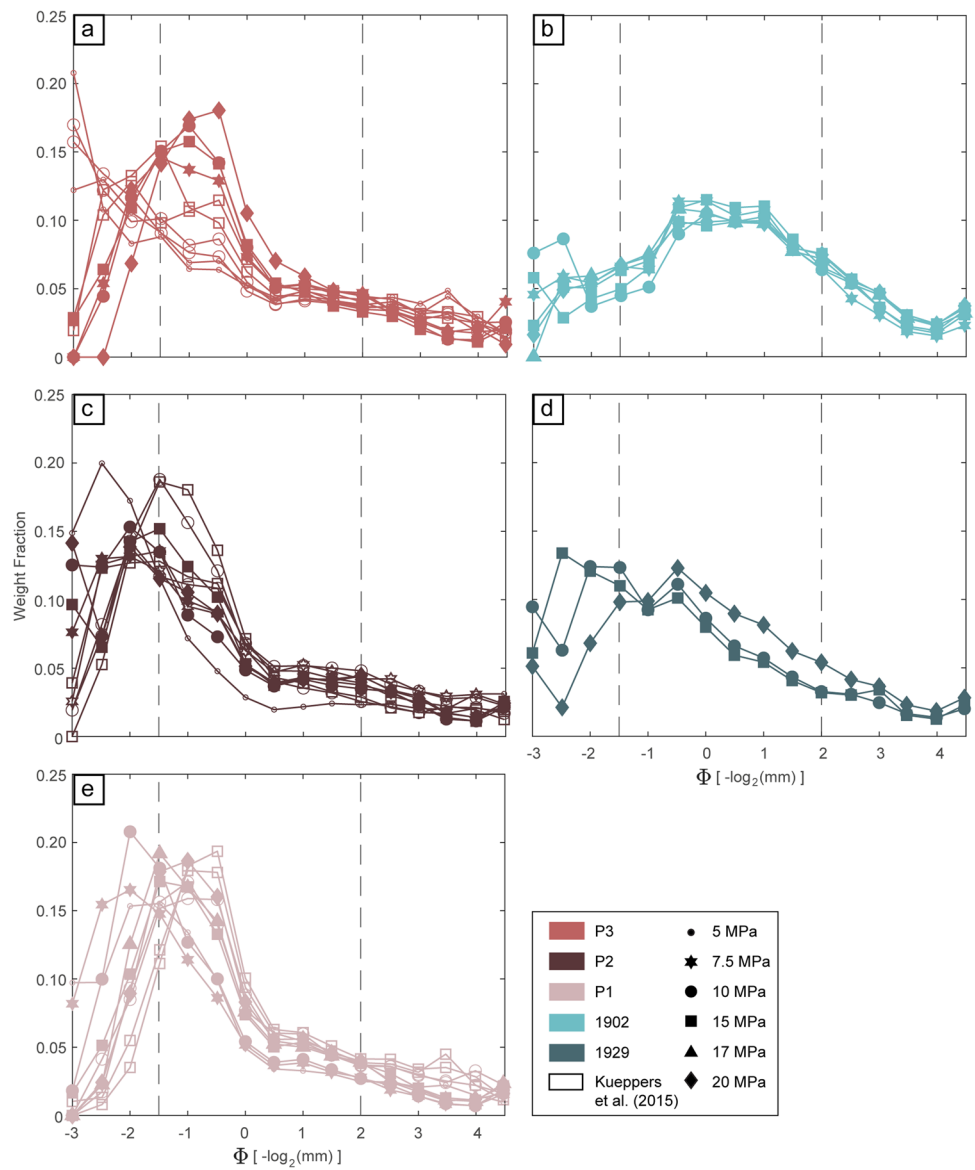
Fig. 9 The fractal dimension of cumulative weight fractions ($D_{f,CW}$) plotted against potential energy of fragmentation (PEF), for Plinian eruptions (**a**) and Peléan eruptions (**b**)
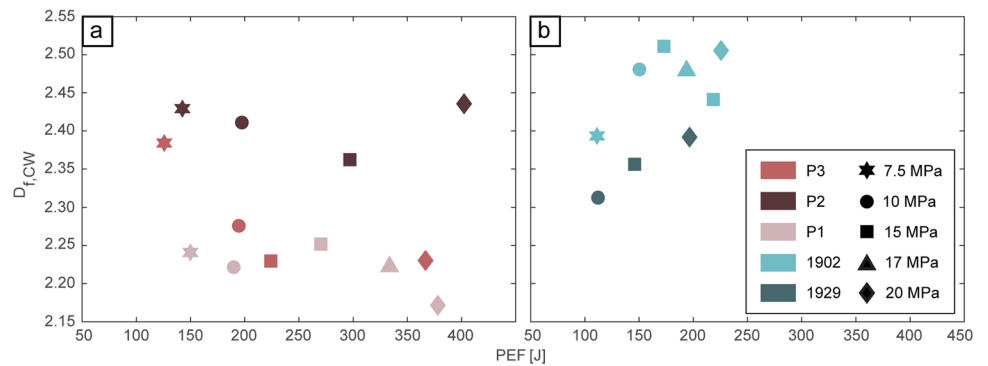
Fragmentation efficiency

We observed a noticeable reduction in the mechanical strength of samples from the same stratigraphic unit related to the microclimate, i.e., samples collected at the rainy side of the volcano (east) were consistently weaker. Heap et al. (2022) reported similar results, observing the tensile strength of volcanic rocks to decrease as a function of extent of hydrothermal alteration. The P2 and P3 samples collected from the eastern side of the volcano (sites 95 and 114 in Fig. 1) exhibit a wider porosity range (Fig. 4) and a higher fragmentation efficiency (Table 1) than their counterparts

from the western side (sites 13 and 209). These samples fragmented inconsistently and differently than typical for juvenile material (Spieler et al. 2004), with some experiments generating more coarse fragments than dry-side counterparts and therefore different GSDs (Fig. 8; Kueppers et al. 2015). Exposure to larger precipitation volumes and presumably greater soil humidity likely correlated with increased weathering, involving breakdown of matrix glass and sufficient structural weakening to influence fragmentation behavior (see also, for example, Mayer et al. 2015). As only juvenile material is relevant for this study, our discussion below is restricted to the behavior and characteristics of the

Fig. 10 Grain size distributions shown as weight fractions across the negative base-two logarithm of sieve aperture. Results of 10 and 20 MPa fragmentation experiments are superimposed for ease of comparison across eruption group materials. Data has been renormalized to exclude $\Phi_2 = -3$, and vertical dashed lines indicate the limits of the analyzed data range
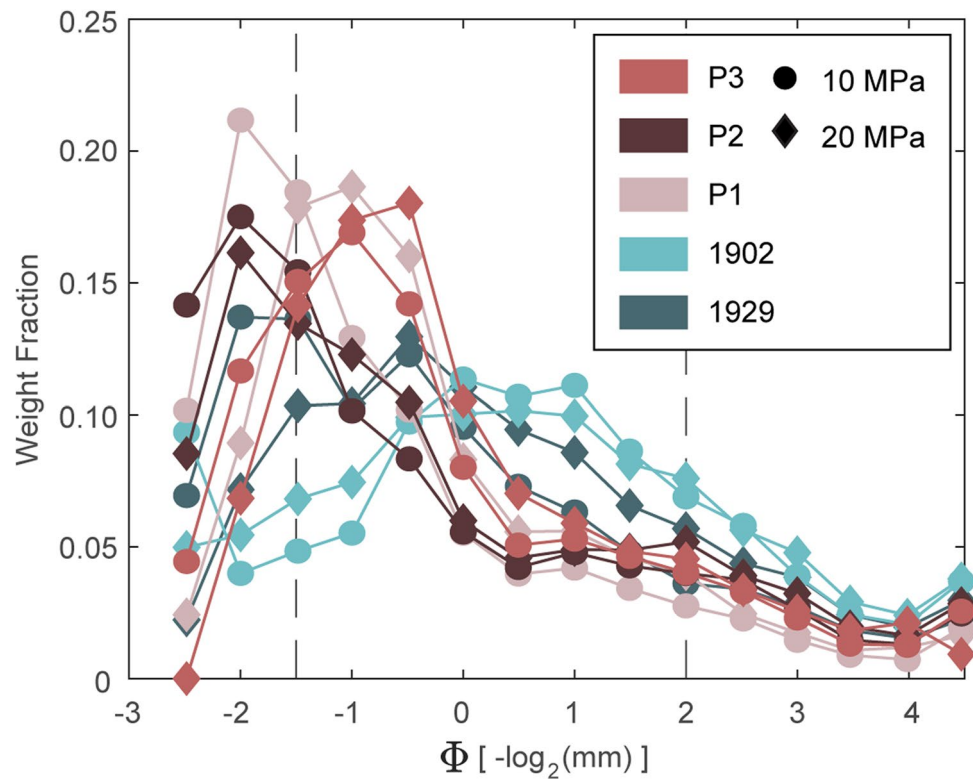
Fig. 11 The fractal dimension of experimental results on materials from Mt. Pelée from this study, together with results for Popocatépetl (Mexico) and Unzen (Japan) materials (*) from Perugini and Kueppers (2012), compared with potential energy of fragmentation (**a**) and open porosity (**b**)
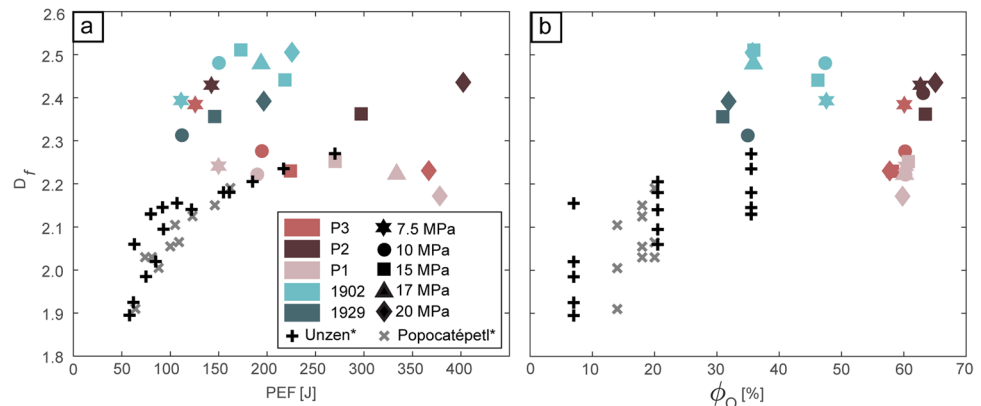
materials collected in 2019 on the dry side. Future sampling activities are planned for tailored textural and geochemical analysis of clasts collected from outcrops in different microclimates from the same stratigraphic units, to explore variability in weathering and devitrification.

Experimental GSD results are distinct between the Plinian and Peléan material groups and internally consistent within results for each considered eruption (Fig. 8), indicating that textural parameters have a greater control on fragmentation efficiency than the overpressure applied. For comparison between material groups, the GSD results of 10 and 20 MPa experiments for each unit are overlain in Fig. 10. This figure was generated following re-normalization to exclude the variation at $\Phi_2 = -3$ observed in Fig. 8, which occurs well outside the defined range of significance indicated by the vertical dashed lines. The 1902 sample experiments produced greater weight fractions of sub-millimeter fines than all other experiments (Fig. 10) and as a group exhibited the most efficient fragmentation (Fig. 9). The 1902 and 1929 samples show a generally positive correlation of $D_{f,\,CW}$ with PEF (Fig. 9) and extend the observed correlation between PEF and fractal dimension of Kueppers et al. (2006a) and Perugini and Kueppers (2012) (Fig. 11a). For these materials, the proportion of fines tends to increase as a function of overpressure. This relationship may be bolstered by more populous crystal cleavage faces providing locations where brittle failure can more easily occur (Cordonnier et al. 2012; Wadsworth et al. 2018). The observed large(r) variability in $D_{f,\,CW}$ results for 1902 samples likely reflects the overall larger textural heterogeneity, including the presence of magmatic enclaves of various sizes. Nonetheless, we are convinced that the presented results point toward a positive correlation of $D_{f,\,CW}$ with PEF. In extrapolating to Peléan eruptions, we can infer that increased overpressurization of a dome system or shallow subsurface magma can lead to enhanced fine-ash production following dome failure or eruption onset. With increased proportions of ash (i.e., relative to larger pyroclasts), heat transfer efficiency increases and PDCs become more buoyant and less topographically confined, increasing the size of the impacted hazard region (e.g., Taddeucci and Palladino 2002 and Wright et al. 2016). During the 1902 eruption of Mt. Pelée, generation of devastating dilute pyroclastic surges (i.e., rather than denser and coarser PDCs) was likely caused by the interplay of particular magma textures and pressure conditions.

In contrast, results from the P1–P3 experiments reveal a sub-horizontal regression in the $D_{f,\,CW}$-PEF relationship, wherein additional overpressure did not result in enhanced disintegration of the starting sample. It seems that for the Martinique samples investigated, there is a maximum value of $D_{f,\,CW}$ that cannot be overcome by magmatic fragmentation alone (Fig. 11a). This cannot be attributed to permeability in porous rocks only, as no significant variation of permeability exists across the starting rock cylinders. Fragmentation by rapid decompression is a multi-step fracture process where the cylinders are broken into initially larger clasts (disrupted by unloading and gas overpressure) which may then break up into finer clasts in subsequent steps. In this case, the distance that gas has to flow through the permeable network to reach the outside of the just-generated clasts is reduced. We speculate that this syn-fragmentation gas loss is dictated by textural characteristics (e.g., porosity, tortuosity, pore throat aperture, and vesicle size distribution) and leads to no apparent fragmentation efficiency changes despite increasing the starting gas pressure (Fig. 11b). Eventually, this gas loss would accommodate the starting pressure in individual experiments and explain the lack of correlation between starting pressure or potential energy and grain size characteristics.

Although the impact on fragmentation was found to be minor, excess potential energy still contributed to acceleration of particles for samples with porosity above the observed threshold (Supplementary Information; Huebsch et al. 2023). Particle ejection begins while the gas jet is still under-expanded and condensed at the vent, impeding precise quantification of the ejection velocity of the first particles. Still, tracking of first visible particles supports that peak ejection velocity tends to be greater for Plinian than Peléan fragments, likely due to higher starting potential energy for equivalent starting pressures. In addition to further quantitative textural characterization, future work will examine componentry of experimentally produced size fractions, to investigate possible concentration of denser materials (e.g., mafic enclaves and phenocrysts) in certain size fractions and if this could bias GSD and fractal dimension results.

Though representing the same process, D_f calculated using cumulative weight fractions cannot be directly compared with that from numbers of particles, because it is a dimensionless parameter. Due to the power law formula being derived for changing grain sizes (Turcotte 1992), from the cubic proportionality of volume and mass, $D_{f,\,CW}$ can only be smaller than 3 (Perugini and Kueppers 2012). Using the Carazzo et al. (2012, 2019, 2020) field TGSD results for fallout deposits from P1, P2, and P3, respectively, we have determined $D_{f,\,CW}$ of 2.6, 2.5, and 2.8, respectively, for particles coarser than negative cumulative weight-grain size slope inflection observed in each (at 0.5 mm for P1 and P3 and 2 mm for P2). As each unique fragmentation process may be described by a single fractal dimension (e.g., Turcotte 1986), or slope, these slope inflections indicate that secondary processes have modified the distribution of grain sizes at some point following primary fragmentation. The fragmentation efficiencies indicated by these field TGSDs are markedly more pronounced than our corresponding experimental results for materials from the same eruptions, especially for P1 and P3. This indicates that secondary fragmentation, despite these field TGSD analyses being of fall and not ignimbrites, outcompetes the opposing processes of washout of fines from rainfall and loss of fines to the ocean, to create an apparent net

increase in fragmentation efficiency. For further comparison of our experimental results and the corresponding field results of Carazzo et al. (2012, 2019, 2020), as well as the number of particles and cumulative weight fraction methods of calculating the fractal dimension, see the Supplementary Information (Huebsch et al. 2023).

Our experimental conditions cause predominantly tensile fractures (primary fragmentation). Particle-setup and particle-particle interactions are of low energy, and the impinging energy of the generated jets to the top of the low-P section is minimized by adding shock-absorbing materials. Future work should aim at constraining post-fragmentation processes (i.e., secondary fragmentation and sorting). To this end, tumbling experiments (Kueppers et al. 2012; Hornby et al. 2020) with polymodal starting material could reveal the dynamic grain size evolution of PDCs after fragmentation and before sedimentation. Furthermore, more detailed field characterization of the TGSD of the Peléan deposits of Mt. Pelée, extending the work of Carazzo et al. (2012, 2019, 2020) on the recent Plinian deposits, would help link deposit characteristics to empirically constrained material response laws (Alidibirov and Panov 1998; Spieler et al. 2004; Kueppers et al. 2006a; Perugini and Kueppers 2012). Experimental GSD data are useful as a calibration tool when interpreting field TGSD results. To improve validity of comparison across experimental and field studies, continued development of TGSD methodology is required, along with the application of a harmonized approach for summarizing fragmentation efficiency.

Conclusions

The Peléan samples analyzed in this study have irregular vesicle shapes and are denser and more crystalline than Plinian samples. This set of textural characteristics indicates more extensive outgassing and crystallization, consistent with the typically lower ascent velocities observed for Peléan eruptions than for Plinian eruptions. Consistent andesitic whole rock and rhyolitic matrix glass compositions demonstrate that magma composition does not significantly vary across eruptive units.

Our experimental results show a porosity threshold, above which applying higher overpressure no longer enhances fragmentation efficiency. Beyond this threshold, which is exceeded here by Plinian samples, gas loss through a permeable network of bubbles and cracks allowed for syn-fragmentation dissipation of potential energy. To further explore this phenomenon, future research should include further textural characterization of samples (e.g., vesicle tortuosity and crystal size distributions) prior to their fragmentation in rapid decompression experiments.

For the investigated lower porosity Peléan materials, fragmentation efficiency was found to increase in experiments with higher applied pressure. This experimentally determined relationship has implications for Peléan eruption hazard assessment: changes in overpressure conditions in this eruptive regime influence the proportion of fines produced and resulting PDC dynamics. The mass fatalities at Mt. Pelée in May of 1902, in regions largely unreachable by dense pyroclastic flows, likely resulted from a specific combination of magma texture and overpressure conditions being met, facilitating production of less topographically controlled, dilute, and ash-rich PDCs.

Our experimental results support that field TGSDs, including those for the three most recent Plinian eruptions of Mt. Pelée, reflect particle and deposit modification by secondary processes. As rapid decompression experiments allow for quantification of the isolated efficiency of primary fragmentation, their results can aid more robust interpretation of fractal dimensions of field deposits comprising texturally comparable material.

Under the assumption that the investigated samples (bomb-sized clasts > 10 cm diameter) are texturally and chemically representative of the juvenile magma involved in these five explosive eruptions, our results confirm the clear correlation between starting conditions of explosive eruptions and the related deposits. Despite their only being preserved in proximal deposits, we wish to stress the probable importance of the comparison of the textural properties of lapilli clasts in future studies. The results presented are nevertheless an important step toward quantitatively revealing the energy underlying explosive eruptions.

Author contribution Conception and design of the study were a collaboration of Kueppers, Huebsch, and Carazzo. Sample collection was performed by Huebsch, Kueppers, Carazzo, and Michaud-Dubuy, with the support of Lejeune. Experiments were performed by Huebsch and Kueppers. Petrophysical characterization was performed by Huebsch, Kueppers, Cimarelli, Hess, Hornby, Weller, and Heap. Analysis was carried out by Huebsch. Data was discussed by Huebsch, Kueppers, Carazzo, Michaud-Dubuy, Perugini, and Dingwell. The first draft of the manuscript was written by Huebsch, and all authors read and approved the final manuscript.

Declarations

We confirm that the first author, Mila Huebsch, and all co-authors of this submission to the Bulletin of Volcanology, have no affiliations with or involvement in any organization or entity with any financial interest. There are no conflicts of interest.

References

Alatorre-Ibargüengoitia MA, Scheu B, Dingwell DB (2011) Influence of the fragmentation process on the dynamics of Vulcanian eruptions. An experimental approach. Earth Planet Sci Lett 302:51–59. https://doi.org/10.1016/j.epsl.2010.11.045

Alidibirov M, Dingwell DB (1996a) An experimental facility for the investigation of magma fragmentation by rapid decompression. Bull Volcanol 58(5):411–416. https://doi.org/10.1007/s004450050149

Alidibirov M, Dingwell DB (1996b) Magma fragmentation by rapid decompression. Nature. https://doi.org/10.1038/380146a0

Alidibirov M, Panov V (1998) Magma fragmentation dynamics: experiments with analogue porous low-strength material. Bull Volc 59(7):481–489. https://doi.org/10.1007/s004450050205

Åstrom JA, Ouchterlony F, Linna RP, Timonen J (2004) Universal dynamic fragmentation in D dimensions. Phys Rev Lett 92(24):1–4. https://doi.org/10.1103/PhysRevLett.92.245506

Aubry T, Engwell S, Bonadonna C, Carazzo G, Scollo S, Van Eaton AR, Taylor IA, Jessop D, Eychenne J, Gouhier M, Mastin LG, Wallace KL, Biass S, Bursik M, Grainger RG, Jellinek AM, Schmidt A (2021) The independent Volcanic Eruption Source Parameter Archive (IVESPA, version 1.0): a new observational database to support explosive eruptive column model validation and development. J Volcanol Geotherm Res:107295. https://doi.org/10.1016/j.jvolgeores.2021.107295

Bérard B, Kieffer G, Raynal JP, Vernet G (2003) Les éruptions volcaniques de la Montagne Pelée et le premier peuplement de la Martinique. In book: Actes du XIXè Congrés international d'Archéologie de la CaraïbeEdition: Publication of the Museo Archeologico Arube vol. 9 Chapter: Volume II Publisher: The Government of Aruba – from https://www.researchgate.net/publication/274372547_Les_eruptions_volcaniques_de_la_Montagne_Pelee_et_le_premier_peuplement_de_la_Martinique

Bonadonna C, Houghton BF (2005) Total grain-size distribution and volume of tephra-fall deposits. Bull Volcanol 67:441–456. https://doi.org/10.1007/s00445-004-0386-2

Boudon G, Le Friant A, Villemant B, Viode J P (2005) Martinique. In Volcanic Hazard Atlas of the Lesser Antilles (ed. J.M. Lindsay, R.E.A. Robertson, J.B. Sheperd and S. Ali), p127-146. Seismic Research Unit, The University of the West Indies, Trinidad and Tobago, W.I.

Bourdier JL, Boudon G, Gourgaud A (1989) Stratigraphy of the 1902 and 1929 nuée-ardente deposits, Mt. Pelée, Martinique. J Volcanol Geotherm Res 38(1-2):77–96. https://doi.org/10.1016/0377-0273(89)90031-0

Brown GM, Holland JG, Sigurdsson H, Tomblin JF, Arculus RJ (1997) Geochemistry of the Lesser Antilles volcanic island arc. Geochim Cosmochim Acta 41(6):785–801. https://doi.org/10.1016/0016-7037(77)90049-7

Brunet M, Le Friant A, Boudon G, Lafuerza S, Talling P, Hornbach M, Ishizuka O, Lebas E, Guyard H, IODP Expedition 340 Science Party (2016) Composition, geometry, and emplacement dynamics of a large volcanic island landslide offshore Martinique: from volcano flank-collapse to seafloor sediment failure? Geochem Geophys Geosyst 17:699-724. https://doi.org/10.1002/2015GC006034

Carazzo G, Kaminski E, Tait S (2008) On the dynamics of volcanic columns: a comparison of field data with a new model of negatively buoyant jets. J Volcanol Geotherm Res 178(1):94–103. https://doi.org/10.1016/j.jvolgeores.2008.01.002

Carazzo G, Tait S, Kaminski E (2019) Marginally stable recent Plinian eruptions of Mt. Pelée volcano (Lesser Antilles): the P2 AD 280 eruption. Bull Volcanol 81(1):1–17. https://doi.org/10.1007/s00445-018-1265-6

Carazzo G, Tait S, Kaminski E, Gardner JE (2012) The recent Plinian explosive activity of Mt. Pelée volcano (Lesser Antilles): the P1 AD 1300 eruption. Bull Volcanol 74:2187–2203. https://doi.org/10.1007/s00445-012-0655-4

Carazzo G, Tait S, Michaud-Dubuy A, Fries A, Kaminski E (2020) Transition from stable column to partial collapse during the 79 cal CE P3 Plinian eruption of Mt Pelée volcano (Lesser Antilles). J Volcanol Geotherm Res 392:106764. https://doi.org/10.1016/j.jvolgeores.2019.106764

Casas AS, Hornby A, Poetsch C, Cimarelli C, Dingwell DB (2022) A novel method for the quantitative morphometric characterization of soluble salts on volcanic ash. Bull Volcanol 84:3. https://doi.org/10.1007/s00445-021-01519-3

Cigala V, Kueppers U, Peña Fernández JJ, Taddeucci J, Sesterhenn J, Dingwell DB (2017) The dynamics of volcanic jets: temporal evolution of particles exit velocity from shocktube experiments. J Geophys Res Solid Earth 122:6031–6045. https://doi.org/10.1002/2017JB014149

Cigala V, Kueppers U, Peña Fernández JJ, Dingwell DB (2021) Linking gas and particle ejection dynamics to boundary conditions in scaled shock-tube experiments. Bull Volcanol 83(8):1-17. 0.1007/s00445-021-01473-0

Colo' L, Ripepe M, Gurioli L, Harris AJ (2020) Fragmentation processes during Strombolian explosions revealed using particle size distribution mapping. Front Earth Sci 8(August):1–10. https://doi.org/10.3389/feart.2020.00356

Cordonnier B, Caricchi L, Pistone M, Castro J, Hess K-U, Gottschaller S, Manga M, Dingwell DB, Burlini L (2012) The viscous-brittle transition of crystal-bearing silicic melt: direct observation of magma rupture and healing. Geol 40:611–614. https://doi.org/10.1130/G3914.1

Costa A, Pioli L, Bonadonna C (2016) Assessing tephra total grain-size distribution: insights from field data analysis. Earth Planet Sci Lett 443:90–107. https://doi.org/10.1016/j.epsl.2016.02.040

Dingwell DB (1996) Volcanic dilemma: flow or blow? Sci 273(5278):1054–1055. https://doi.org/10.1126/science.273.5278.1054

Dupuy C, Dostal J, Traineau H (1985) Geochemistry of volcanic rocks from Mt. Pelée, Martinique. J Volcanol Geotherm Res 26:147–165. https://doi.org/10.1016/0377-0273(85)90050-2

Farquharson JI, Heap MJ, Lavallée Y, Varley NR, Baud P (2016) Evidence for the development of permeability anisotropy in lava domes and volcanic conduits. J Volcanol Geotherm Res 323:163–185. https://doi.org/10.1016/j.jvolgeores.2016.05.007

Fichaut M, Maury RC, Traineau H, Westercamp D, Joron JL, Gourgaud A, Coulon C (1989) Magmatology of Mt. Pelée (Martinique, F.W.I.). III: fractional crystallization versus magma mixing. J Volcanol Geotherm Res 38(1-2):189–213. https://doi.org/10.1016/0377-0273(89)90037-1

Germa A, Lahitte P, Quidelleur X (2015) Construction and destruction of Mont Pelée volcano: volumes and rates constrained from a geomorphological model of evolution. J Geophys Res Earth Surf 120:1206–1226. https://doi.org/10.1002/2014JF003355

Germa A, Quidelleur X, Lahitte P, Labanieh S, Chauvel C (2011) The K-Ar Cassignol-Gillot technique applied to western Martinique lavas: a record of Lesser Antilles arc activity from 2 Ma to Mount Pelée volcanism. Quat Geochronol 6:341–355. https://doi.org/10.1016/j.quageo.2011.02.001

Gilvarry JJ, Bergstrom BH (1961) Fracture of brittle solids. II. Distribution function for fragment size in single fracture (experimental). J Appl Phys 32(3):400–410. https://doi.org/10.1063/1.1736017

Gourgaud A, Fichaut M, Joron JL (1989) Magmatology of Mt. Pelée (Martinique, F.W.I.). I: magma mixing and triggering of the 1902 and 1929 Pelean nuées ardentes. J Volcanol Geotherm Res 38:143–169. https://doi.org/10.1016/0377-0273(89)90035-8

Gueugneau V, Kelfoun K, Charbonnier S, Germa A, Carazzo G (2020) Dynamics and impacts of the May 8th, 1902 pyroclastic current at Mount Pelée (Martinique): new insights from numerical modeling. Front Earth Sci 8:279. https://doi.org/10.3389/feart.2020.00279

Haug ØT, Galland O, Gisler GR (2013) Experimental modelling of fragmentation applied to volcanic explosions. Earth Planet Sci Lett 384:188–197. https://doi.org/10.1016/j.epsl.2013.10.004

Heap MJ, Kennedy BM (2016) Exploring the scale-dependent permeability of fractured andesite. Earth Planet Sci Lett 447:139–150. https://doi.org/10.1016/j.epsl.2016.05.004

Heap MJ, Kushnir AR, Gilg HA, Wadsworth FB, Reuschlé T, Baud P (2017) Microstructural and petrophysical properties of the Permo-Triassic sandstones (Buntsandstein) from the Soultz-sous-Forêts geothermal site (France). Geothermal Energy 5(1):1–37. https://doi.org/10.1186/s40517-017-0085-9

Heap MJ, Harnett CE, Wadsworth FB, Gilg HA, Carbillet L, Rosas-Carbajal M, Komorowski JC, Baud P, Troll VR, Deegan FM, Holohan EP (2022) The tensile strength of hydrothermally altered volcanic rocks. J Volcanol Geotherm Res 428:107576. https://doi.org/10.1016/j.jvolgeores.2022.107576

Holzmueller J, Kueppers U (2015) Impinging jet experiments on samples from the P3 eruption of Mt. Pelée, Martinique. Unpublished data set.

Hornby A, Kueppers U, Maurer B, Poetsch C, Dingwell D (2020) Experimental constraints on volcanic ash generation and clast morphometrics in pyroclastic density currents and granular flows. Volcanica 3(2):263–283. https://doi.org/10.30909/vol.03.02.263283

Hornby A (2022) RockPie (v1.2). Zenodo. https://doi.org/10.5281/zenodo.7109054

Huebsch M, Kueppers U, Carazzo G, Cimarelli C, Hess KU, Hornby A, Lejeune AM, Dubuy A, Perugini D, Weller D, Heap MJ, Dingwell DB (2023) Dataset of experimental fragmentation results and petrophysical properties for pyroclasts from Mt. Pelée, Martinique. GFZ Data Services. https://doi.org/10.5880/fidgeo.2023.030

Kaminski E, Jaupart C (1998) The size distribution of pyroclasts and the fragmentation sequence in explosive volcanic eruptions. J Geophys Res Solid Earth 103:29759–29779. https://doi.org/10.1029/98jb02795

Korvin G (1992) Fractal models in the earth sciences. 396. Elsevier Amsterdam

Kueppers U, Perugini D, Dingwell DB (2006a) "Explosive energy" during volcanic eruptions from fractal analysis of pyroclasts. Earth Planet Sci Lett 248:800–807. https://doi.org/10.1016/j.epsl.2006.06.033

Kueppers U, Scheu B, Spieler O, Dingwell DB (2006b) Fragmentation efficiency of explosive volcanic eruptions: a study of experimentally generated pyroclasts. J Volcanol Geotherm Res 153(1-2):125–135

Kueppers U, Putz C, Spieler O, Dingwell DB (2012) Abrasion in pyroclastic density currents: insights from tumbling experiments. Phys Chem Earth 45-46:33–39. https://doi.org/10.1016/j.pce.2011.09.00

Kueppers U, Uhlig J, Carazzo G, Kaminski E, Perugini D, Tait S, Clouard V (2015) The three youngest Plinian eruptions of Mt Pelée, Martinique (P1 , P2 and P3): constraining the eruptive conditions from field and experimental studies. In: EGU General Assembly Conference Abstracts, vol 17, pp 2082–2082

Kueppers U, Pimentel A, Ellis B, Forni F, Neukampf J, Pacheco J, Perugini D, Queiroz G (2019) Biased volcanic hazard assessment due to incomplete eruption records on ocean islands: an example of Sete Cidades Volcano, Azores. Front Earth Sci 7:122. https://doi.org/10.3389/feart.2019.00122

Lacroix A (1904) La Montagne Pelée et ses éruptions. Masson, Paris

Le Friant A, Boudon G, Deplus C, Villemant B (2003) Large-scale flank collapse events during the activity of Montagne Pelée, Martinique, Lesser Antilles. J Geophys Res 108(B1):1–15. https://doi.org/10.1029/2001jb001624

Liu EJ, Cashman KV, Rust A (2015) Optimising shape analysis to quantify volcanic ash morphology. GeoResJ 8:14–30. https://doi.org/10.1016/j.grj.2015.09.001

Macdonald R, Hawkesworth CJ, Heath E (2000) The Lesser Antilles volcanic chain: a study in arc magmatism. Earth Sci Rev 49:1–76. https://doi.org/10.1016/S0012-8252(99)00069-0

Mandelbrot BB (1983) The Fractal Geometry of Nature. WH Freeman, New York

Martel C, Bourdier JL, Pichavant M, Traineau H (2000) Textures, water content and degassing of silicic andesites from recent Plinian and dome-forming eruptions at Mount Pelée volcano (Martinique, Lesser Antilles arc). J Volcanol Geotherm Res 96(3-4):191–206. https://doi.org/10.1016/S0377-0273(99)00147-X

Martel C, Pichavant M, Bourdier JL, Traineau H, Holtz F, Scaillet B (1998) Magma storage conditions and control of eruption regime in silicic volcanoes: experimental evidence from Mt. Pelée. Earth Planet Sci Lett 156(1-2):89–99. https://doi.org/10.1016/s0012-821x(98)00003-x

Martel C, Poussineau S (2007) Diversity of eruptive styles inferred from the microlites of Mt Pelée andesite (Martinique, Lesser Antilles). J Volcanol Geotherm Res 166(3-4):233–254. https://doi.org/10.1016/j.jvolgeores.2007.08.003

Mayer K, Scheu B, Gilg HA, Heap MJ, Kennedy BM, Lavallée Y, Letham-Brake M, Dingwell DB (2015) Experimental constraints on phreatic eruption processes at Whakaari (White Island volcano). J Volcanol Geotherm Res 302:150–162. https://doi.org/10.1016/j.jvolgeores.2015.06.014

Michaud-Dubuy A, Carazzo G, Kaminski E, Girault F (2018) A revisit of the role of gas entrapment on the stability conditions of explosive volcanic columns. J Volcanol Geotherm Res 357:349–361. https://doi.org/10.1016/j.jvolgeores.2018.05.005

Michaud-Dubuy A, Carazzo G, Tait S, Le Hir G, Fluteau F, Kaminski E (2019) Impact of wind direction variability on hazard assessment in Martinique (Lesser Antilles): the example of the 13.5 ka cal BP Bellefontaine Plinian eruption of Mount Pelée volcano. J Volcanol Geotherm Res 381:193–208. https://doi.org/10.1016/j.jvolgeores.2019.06.004

Michaud-Dubuy A, Carazzo G, Kaminski E (2020) Wind entrainment in jets with reversing buoyancy: implications for volcanic plumes. J Geophys Res Solid Earth 125:e2020JB020136. https://doi.org/10.1029/2020JB020136

Michaud-Dubuy A, Carazzo G, Balcone-Boissard H, Boudon G, Kaminski E (2023) Unsuspected explosive activity of Montagne Pelée (Lesser Antilles) during the 25–10 ka period. J Volcanol Geotherm Res 440:107873. https://doi.org/10.1016/j.jvolgeores.2023.107873

Mueller S, Melnik O, Spieler O, Scheu B, Dingwell DB (2005) Permeability and degassing of dome lavas undergoing rapid decompression: An experimental determination. Bull Volc 67(6):526–538. https://doi.org/10.1007/s00445-004-0392-4

Naulin A (2016) Recensement de la population en Martinique - 385 551 habitants au 1er janvier 2013, Insee

Neri A, Dobran F (1994) Influence of eruption parameters on the thermofluid dynamics of collapsing volcanic columns. J Geophys Res 99(B6). https://doi.org/10.1029/94jb00471

Perugini D, Kueppers U (2012) Fractal analysis of experimentally generated pyroclasts: a tool for volcanic hazard assessment. Acta Geophys 60:682–698. https://doi.org/10.2478/s11600-012-0019-7

Pichavant M, Martel C, Bourdier JL, Scaillet B (2002) Physical conditions, structure, and dynamics of a zoned magma chamber: Mount Pelée (Martinique, Lesser Antilles Arc). J Geophys Res 107. https://doi.org/10.1029/2001JB000315

Pioli L, Bonadonna C, Pistolesi M (2019) Reliability of total grain-size distribution of tephra deposits. Sci Rep 9(1):1–15. https://doi.org/10.1038/s41598-019-46125-8

Reckziegel F, Bustos E, Mingari L, Báez W, Villarosa G, Folch A, Collini E, Viramonte J, Romero J, Osores S (2016) Forecasting volcanic ash dispersal and coeval resuspension during the April–May 2015 Calbuco eruption. J Volcanol Geotherm Res 321:44–57. https://doi.org/10.1016/j.jvolgeores.2016.04.033

Romer M (1934) L'éruption de la Montagne Pelée (Martinique) de 1929 à 1933. Ann Phys Globe France Outre Mer 5:129–147

Roobol MJ, Smith AL (1976) Mount Pelée, Martinique: A pattern of alternating eruptive styles. Geol 4(9):521–524. https://doi.org/10.1130/0091-7613(1976)4<521:MPMAPO>2.0.CO;2

Sarkar A, Bhattacharjee D, Chattopadhyay A (2020) Size distribution of survivor clasts in pseudotachylyte and cataclasite: implications for crushing and melting processes in seismic fault zones. J Earth Syst Sci 129(1):1–14. https://doi.org/10.1002/gj.3900

Scheu B, Spieler O, Dingwell DB (2006) Dynamics of explosive volcanism at Unzen volcano: an experimental contribution. Bull Volc 69(2):175–187. https://doi.org/10.1007/s00445-006-0066-5

Schmid M, Kueppers U, Cigala V, Dingwell DB (2022) Complex geometry of volcanic vents and asymmetric particle ejection: experimental insights. Bull Volcanol 84(8):1–18. https://doi.org/10.1007/s00445-022-01580-6

Schmid M, Kueppers U, Cigala V, Sesterhenn J, Dingwell DB (2020) Release characteristics of overpressurised gas from complex vents: implications for volcanic hazards. Bull Volcanol 82(11):1–12. https://doi.org/10.1007/s00445-020-01407-2

Smith A, Roobol M (1990) Mt. Pelée, Martinique; a study of an active island-arc volcano. In: Geological Society of America Memoirs. https://doi.org/10.1130/MEM175-p1

Solaro C, Boudon G, Le Friant A, Balcone-Boissard H, Emmanuel L, Paterne M, Party IES (2020) New insights into the recent eruptive and collapse history of Montagne Pelée (Lesser Antilles Arc) from offshore marine drilling site U1401A (IODP Expedition 340). J Volcanol Geotherm Res 403:107001. https://doi.org/10.1016/j.jvolgeores.2020.107001

Spieler O, Kennedy B, Kueppers U, Dingwell DB, Scheu B, Taddeucci J (2004) The fragmentation threshold of pyroclastic rocks. Earth Planet Sci Lett 226:139–148. https://doi.org/10.1016/j.epsl.2004.07.016

Taddeucci J, Palladino D (2002) Particle size-density relationships in pyroclastic deposits: inferences for emplacement processes. Bull Volcanol 64:273–284. https://doi.org/10.1007/s00445-002-0205-6

Toramaru A, Noguchi S, Oyoshihara S, Tsune A (2008) MND (microlite number density) water exsolution rate meter. J Volcanol Geotherm Res 175(1-2):156–167. https://doi.org/10.1016/j.jvolgeores.2008.03.035

Turcotte DL (1986) Fractals and fragmentation. New York. 91(5):1921–1926

Turcotte DL (1989) Fractals in geology andgeophysics. Pure App Geophys 131:171–196. https://doi.org/10.1007/BF00874486

Turcotte DL (1992) Fractals and chaos in geology and geophysics. Cambridge University Press

Traineau H, Westercamp D, Bardintzeff JM, Miskovsky JC (1989) The recent pumice eruptions of Mt. Pelée volcano, Martinique. Part I: Depositional sequences, description of pumiceous deposits. J Volcanol Geotherm Res 38(1–2):17–33. https://doi.org/10.1016/0377-0273(89)90027-9

Villemant B, Boudon G (1999) H_2O and halogen (F, Cl, Br) behaviour during shallow magma degassing processes. Earth Planet Sci Lett 168:271–286. https://doi.org/10.1016/S0012-821X(99)00058-8

Vincent PM, Bourdier JL, Boudon G (1989) The primitive volcano of Mount Pelée: its construction and partial destruction by flank collapse. J Volcanol Geotherm Res 38(1–2):1–15. https://doi.org/10.1016/0377-0273(89)90026-7

Wadsworth FB, Witcher TW, Vossen C, Hess K-U, Unwin H, Scheu B, Castro JM, Dingwell DB (2018) Combined effusive-explosive silicic volcanism straddles the multiphase viscous-to-brittle transition. Nat Commun 9:4696. https://doi.org/10.1038/s41467-018-07187-w

Westercamp D, Traineau H (1983) The past 5,000 years of volcanic activity at Mt. Pelée Martinique (F.W.I.): implications for assessment of volcanic hazards. J Volcanol Geotherm Res 17:159–185. https://doi.org/10.1016/0377-0273(83)90066-5

Wilson L, Sparks RS, Walker GP (1980) Explosive volcanic eruptions — IV. The control of magma properties and conduit geometry on eruption column behaviour. Geophys J Int 63(1):117–148. https://doi.org/10.1111/j.1365-246X.1980.tb02613.x

Wright JV, Smith AL, Roobol MJ, Mattioli GS, Fryxell JE (2016) Distal ash hurricane (pyroclastic density current) deposits from a ca. 2000 yr B.P. Plinian-style eruption of Mount Pelée, Martinique: distribution, grain-size characteristics, and implications for future hazard. GSA Bull 128(5/6):777–791. https://doi.org/10.1130/B31282.1

Authors and Affiliations

Mila Huebsch[1,2] · **Ulrich Kueppers[1]** · **Guillaume Carazzo[3]** · **Corrado Cimarelli[1]** · **Kai-Uwe Hess[1]** · **Adrian Hornby[4]** · **Anne-Marie Lejeune[5,6]** · **Audrey Michaud-Dubuy[3,7]** · **Diego Perugini[8]** · **Daniel Weller[1]** · **Michael J. Heap[9,10]** · **Donald B. Dingwell[1]**

✉ Mila Huebsch
mila.huebsch@auckland.ac.nz

[1] Department of Earth and Environmental Sciences, Ludwig-Maximilians-Universität (LMU), Munich, Germany

[2] School of Environment, University of Auckland, Auckland, New Zealand

[3] Institut de Physique du Globe de Paris, Université de Paris Cité, Paris, France

[4] Department of Earth and Atmospheric Sciences, Cornell University, Ithaca, NY, USA

[5] Observatoire Volcanologique et Sismologique de Martinique, Institut de Physique du Globe de Paris, Université de Paris Cité, Paris, Martinique, France

[6] Institut des Sciences de la Terre de Paris, Sorbonne Université, Paris, France

[7] Université Clermont Auvergne, CNRS, Institut des Sciences, Clermont-Ferrand, France

[8] Department of Earth Sciences, University of Perugia, Perugia, Italy

[9] Université de Strasbourg, CNRS, Institut Terre et Environnement de Strasbourg, UMR 7063, 5 rue Descartes, F-67084 Strasbourg, France

[10] Institut Universitaire de France (IUF), Paris, France